Supporting information

c-Axis-Oriented sheet-like Cu/AEI zeolite contributed continuous direct oxidative methane to methanol

Peipei Xiao [a] ,Yong Wang [a] , Kengo Nakamura [a], Yao Lu [a] , Junko N. Kondo [a], Hermann Gies [a,b], Toshiyuki Yokoi [a,*]

[a] Institute of Innovative Research, Tokyo Institute of Technology, 4259 Nagatsuta, Midori-ku, Yokohama 226-8503, Japan
[b] Institute of Geology, Mineralogy und Geophysics, Ruhr-University Bochum, Bochum 44780, Germany

* Corresponding authors.
E-mail address: yokoi@cat.res.titech.ac.jp

Characterization of catalysts

XRD pattern was collected on a Rint-Ultima III (Rigaku) using a Cu Kα X-ray source (40 kV, 40 mA).

Elemental analyses of the sample were performed on an inductively coupled plasma-atomic emission spectrometer (ICP-AES, Shimadzu ICPE-9000).

Field-emission scanning electron microscopic (FE-SEM) images of the powder samples were obtained on S-5200 (Hitachi) microscope operating at 1 kV.

Nitrogen adsorption and desorption measurements to obtain information on the micro- and meso-porosities were conducted at -196 °C on a Belsorp-mini II (MicrotracBEL).

Solid-state ^{29}Si and ^{27}Al MAS NMR spectra were measured on a JEOL ECA-600 spectrometer at a resonance frequency of 156.4 MHz using a 4 mm sample rotor with a spinning rate of 15.0 kHz. The ^{29}Si and ^{27}Al chemical shifts were referenced to -34.12 and -0.54 ppm, polydimethylsiloxane (PDMS) and $AlNH_4(SO_4)_2 \cdot 12H_2O$, respectively.

Temperature-programmed ammonia desorption (NH_3-TPD) profiles were recorded on Multitrack TPD equipment (Japan BEL). Typically, 25 mg of catalyst was pretreated at 600 °C in He (50 mL min^{-1}) for 1 h and then cooled to 100 °C. Prior to the adsorption of NH_3, the sample was evacuated at 100 °C for 1 h. Approximately 2500 Pa of NH_3 was allowed to contact with the sample at 100 °C for 10 min. Subsequently, the sample was evacuated to remove weakly adsorbed NH_3 at the same temperature for 30 min. Finally, the sample was cooled to 100 °C and heated from 100 to 600 °C at a ramping rate of 10 °C min^{-1} in a He flow (50 mL min^{-1}). A thermal conductivity detector (TCD) was used to monitor desorbed NH_3. The amount of acid sites was determined by the fitting peak area of the profiles.

UV-vis spectra were collected in the range of 190-600 nm on a V-650DS spectrometer (JASCO). The diffuse reflectance spectra were converted into the absorption spectra using the Kubelka-Munk function.

Fourier Transform Infrared (FTIR) spectra were obtained by using a JASCO 4100 FTIR spectrometer equipped with a triglycine sulfate (TGS) detector. IR spectra of the clean disk were recorded in vacuum at 25 °C to obtain background spectra. The sample was pressed into a self-supporting disk (20 mm diameter, 30−60 mg) and placed in an IR cell attached to a closed-gas circulation system. The sample was pretreated by evacuation at 500 °C for 1 h, and then the temperature was reduced to -120 °C to measure the hydroxyl vibration and follow by adsorption of 5−120 Pa NO or 5−1000 Pa CO at -120 °C. The IR spectra resulting from the subtraction of the background spectra from those with NO or CO adsorbed are shown unless otherwise noted.

Catalytic reaction

The continuous oxidation of methane reaction was performed in a fixed-bed flow reactor. The online-reaction-analysis system was equipped with two six-port inlet valves, as Figure S7 displayed. In each run, 100 mg of catalyst in a granular form (400−600 μm) was charged into a quartz tube (inner diameter 4 mm), which was placed in an electric tube furnace. The catalyst was pretreated at 500 °C for 1 h in an Ar flow. The reaction was conducted at 350 °C in a flowing gas mixture of CH_4, N_2O, H_2O, and Ar with flow rates of 10, 10, 2, and 3 mL·min^{-1} (Figure S8). The outlet gas, containing the products, unreacted CH_4 and N_2O, was analyzed using two on-line gas

chromatographs (GC; GC-2014, Shimadzu). One of the GCs was used with a Shin carbon ST 50/80 packed column (Agilent Technologies, inner diameter 3 mm, length 6 m) and a TCD detector. Specifically, GC-TCD was used to detect H_2, N_2O, CO, CO_2 and CH_4. The other GC was equipped with a Porapak Q 80/100 packed column (Agilent Technologies, inner diameter 3 mm, length 6 m), a flame ionization detector (FID), and a methanizer. The GC-FID was used to investigate CH_4, and the produced methanol (MeOH), dimethyl ether (DME), alkanes, and alkenes. The yield of each carbon-containing product was calculated by considering the number of carbon atoms. The methane conversion in this study was defined as the total obtained products, and calculated as:

$$C_{CH4} = \frac{\sum(i * Ci)}{\sum(i * Ci) + CH4}$$

where C_{CH4} is the CH_4 conversion, i is the number of carbon atoms in product C_i, $\Sigma(i*C_i)$ is the total amount of carbon of all the products, and *CH4* is the amount of CH_4 detected at the same time.

The N_2O conversion was calculated as:

$$C_{N2O} = \frac{ni - na}{ni}$$

where C_{N2O} is the N_2O conversion, n_i is the initial N_2O molar weight, n_a is the N_2O molar weight after reaction.

Note that, CH_4 and N_2O conversion were calculated according to different methods, thus they were not equal in value.

The product selectivity is calculated as:

$$S_{Ci} = \frac{i * Ci}{\sum(i * Ci)}$$

where S_{Ci} is the selectivity of the product C_i, $\Sigma(i*C_i)$ is the total amount of carbon of all the products.

The product yield is calculated as:

$$Y_{Ci} = \frac{i * Ci}{\sum(i * Ci) + CH4}$$

where Y_{Ci} is the yield of the product C_i, $\Sigma(i*C_i)$ is the total amount of carbon of all the products, and *CH4* is the amount of CH_4 detected at the same time.

The products formation rates are calculated as:

$$R_{Ci} = Y_{Ci} * F_{CH4}/m_{cat}$$

where R_{Ci} is the formation rate of product C_i, F_{CH4} is the initial flow rate of CH_4, m_{cat} is the mass of catalyst.

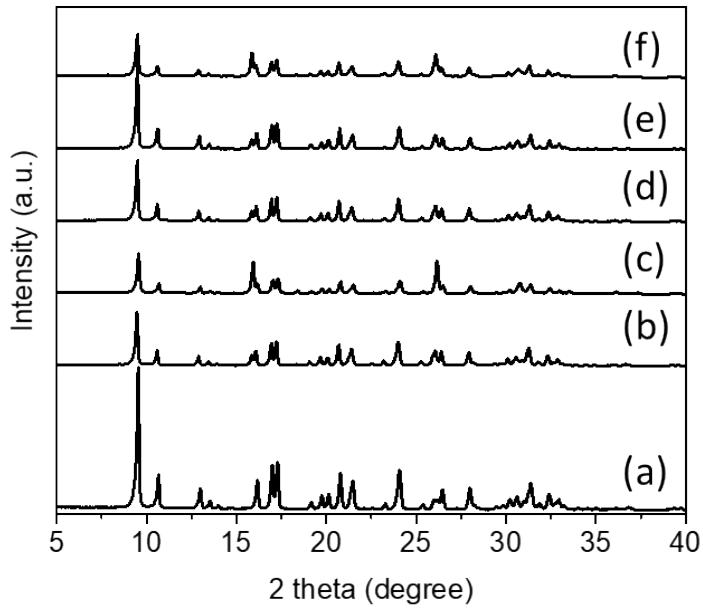

Fig. S1. XRD patterns of (a) refer AEI, (b) H-AEI-C, (c) H-AEI-S, (d) H-AEI-C-700, (e) H-AEI-C-800, (f) H-AEI-S-A-N zeolites.

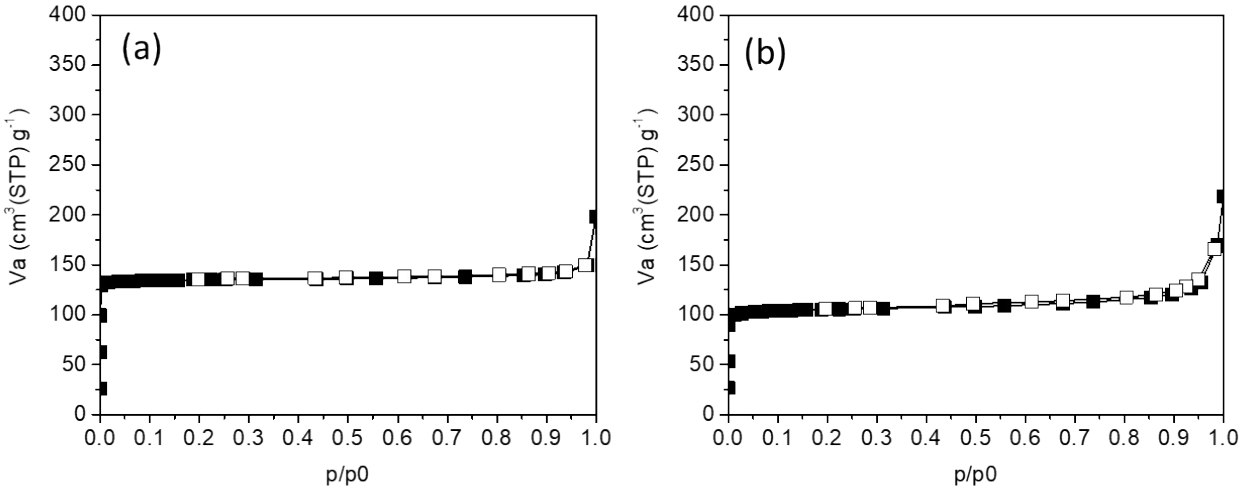

Fig. S2. N_2 adsorption and desorption isotherms of (a) H-AEI-C and (b) H-AEI-S zeolites.

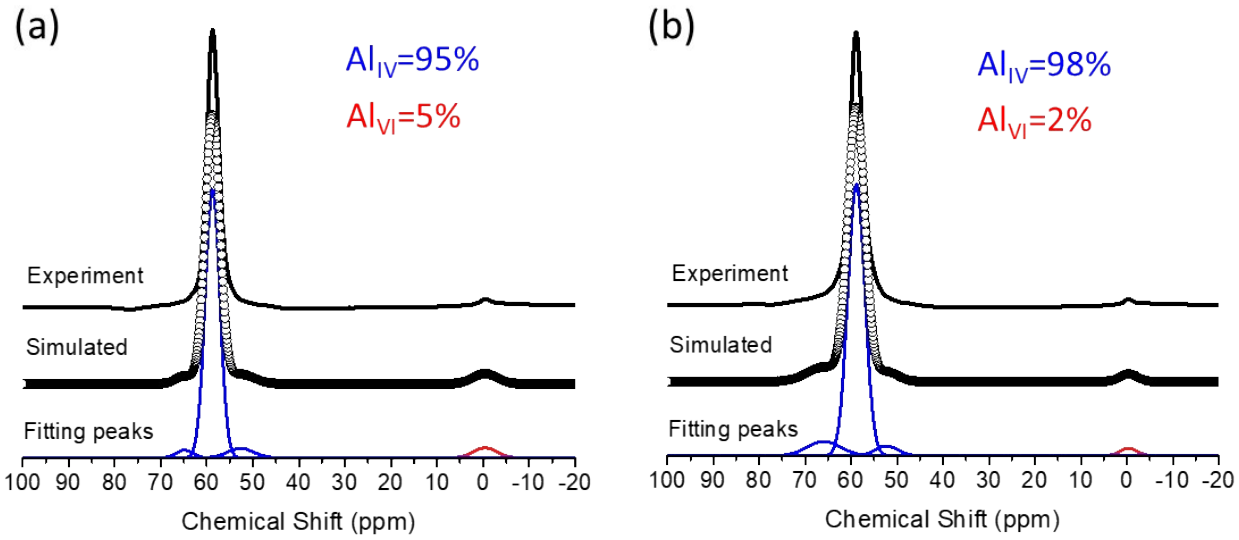

Fig. S3. Deconvolution of ^{27}Al MAS NMR patterns for (a) H-AEI-C and (b) H-AEI-S zeolites.

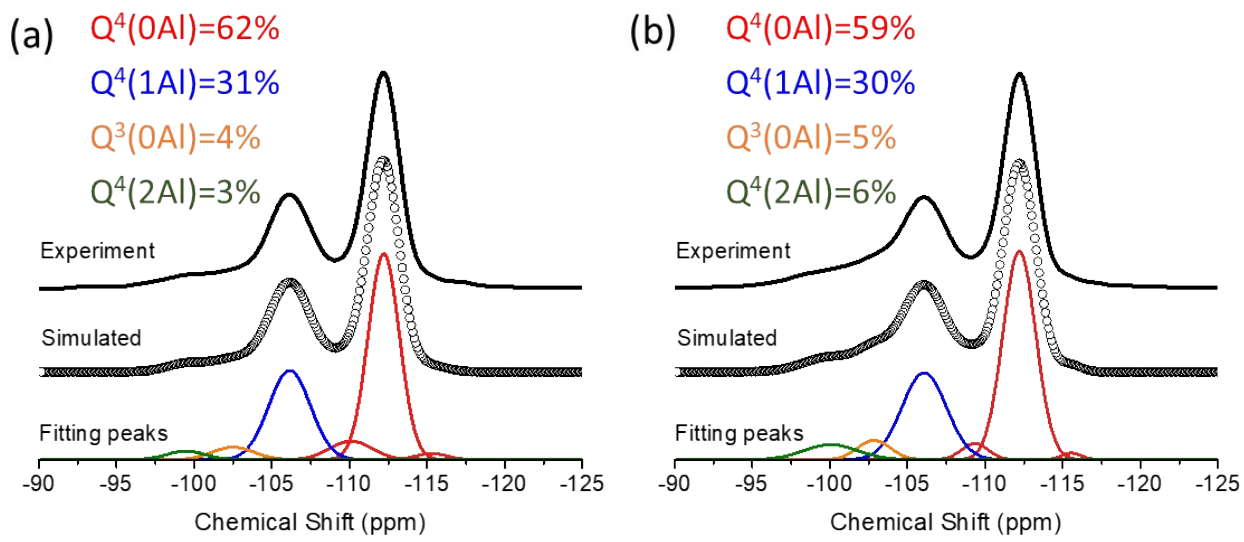

Fig. S4. Deconvolution of ^{29}Si MAS NMR patterns for (a) H-AEI-C and (b) H-AEI-S zeolites

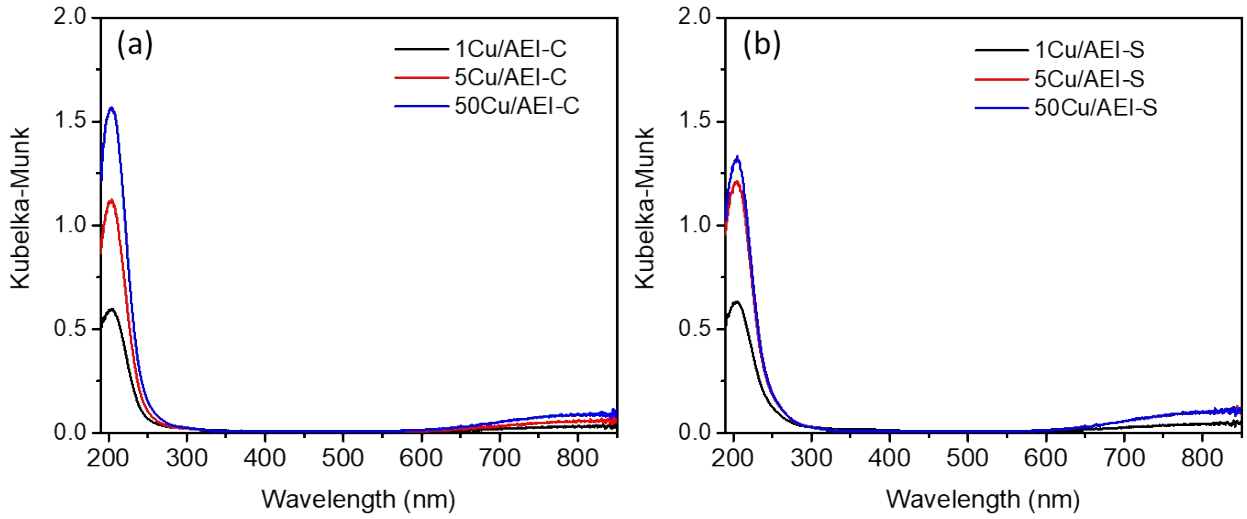

Fig. S5. UV-vis spectra of (a) *x*Cu/AEI-C and (b) *x*Cu/AEI-S zeolite catalysts.

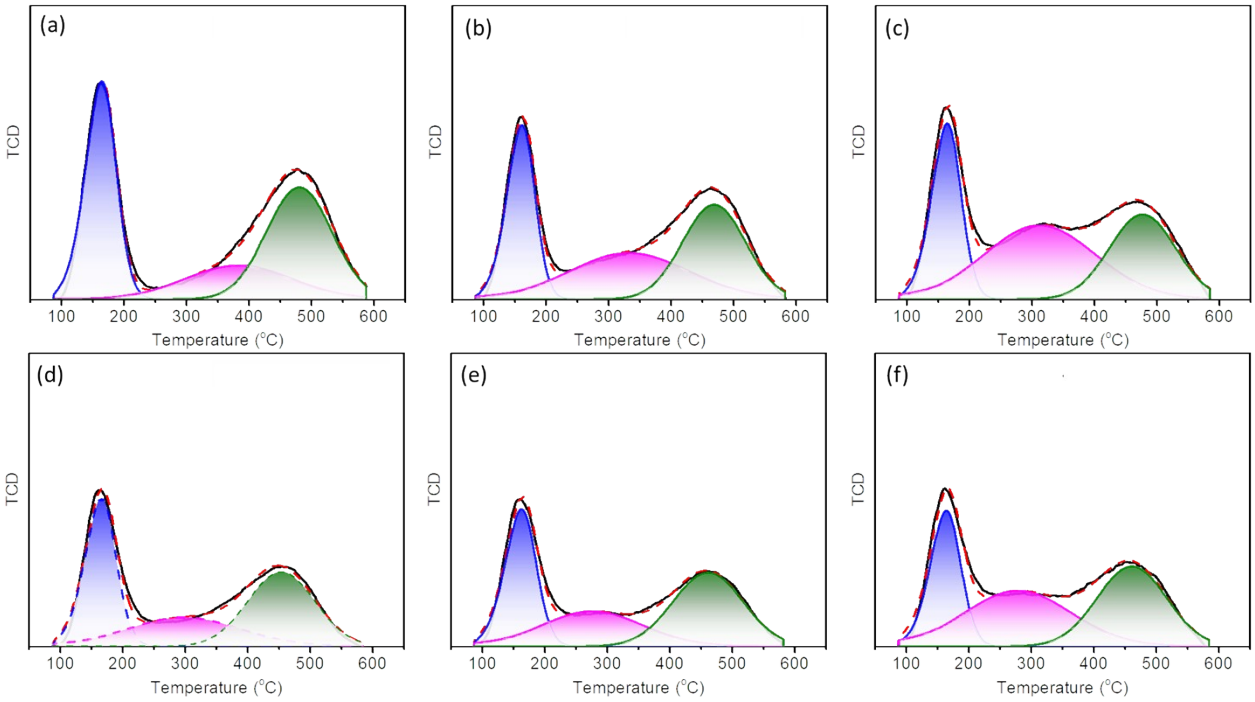

Figure S6. Deconvolution of NH_3-TPD curves of (a) 1Cu/AEI-C, (b) 5Cu/AEI-C, (c) 50Cu/AEI-C, (d) 1Cu/AEI-S, (e) 5Cu/AEI-S, (f) 50Cu/AEI-S zeolite catalysts.

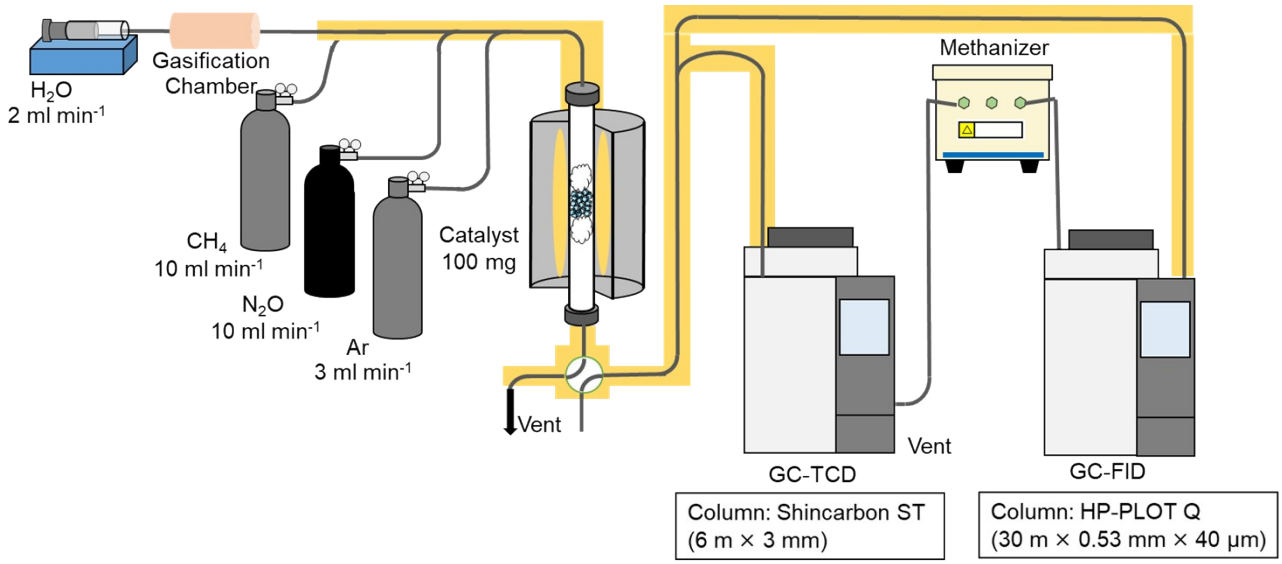

Fig. S7. Schematic diagram of the online-analysis system for continuous direct conversion of methane.

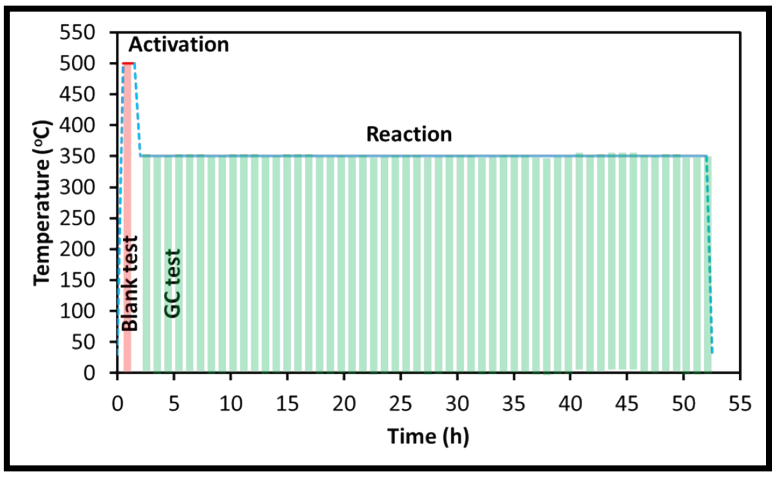

Fig. S8. Temperature program of the continuous oxidation of methane reaction under 350 °C to study the catalytic stability.

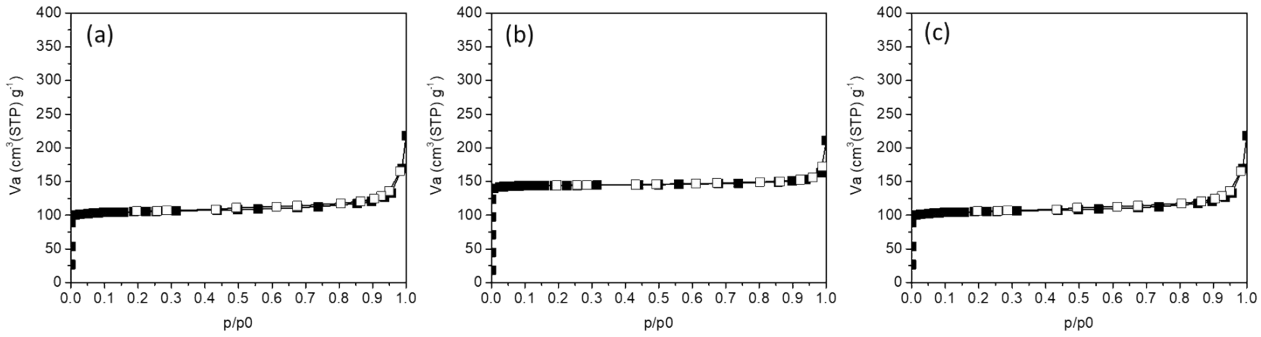

Fig. S9. N_2 adsorption and desorption isotherms of (a) 5Cu/AEI-C-700, (b) 5Cu/AEI-C-800 (c) 5Cu/AEI-S zeolite catalysts.

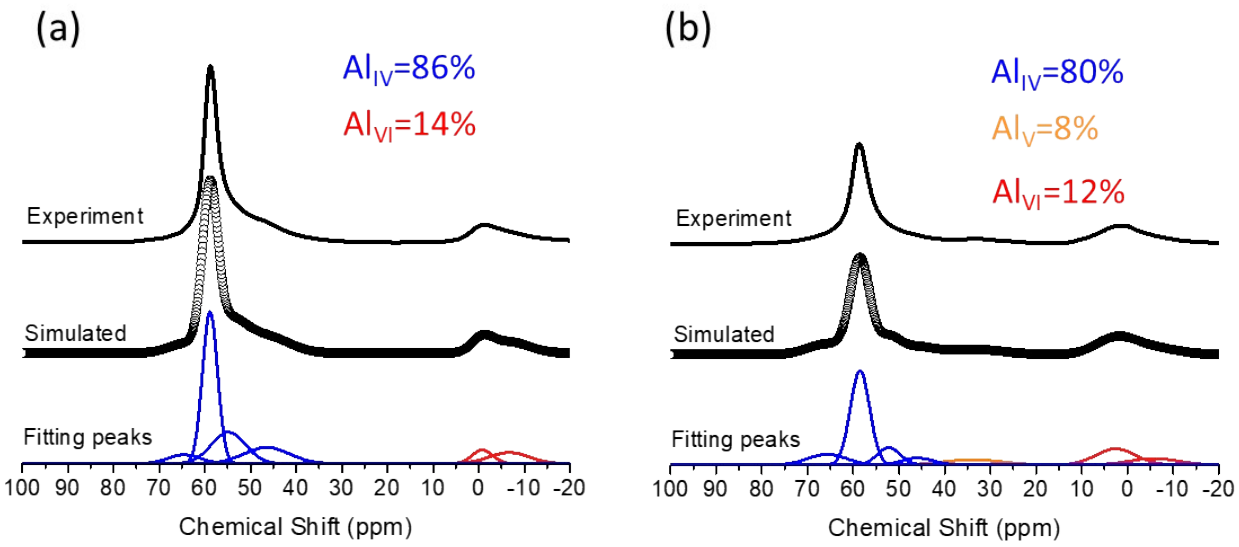

Fig. S10. Deconvolution of ^{27}Al MAS NMR patterns for (a) H-AEI-C-700 and (b) H-AEI-C-800 zeolites.

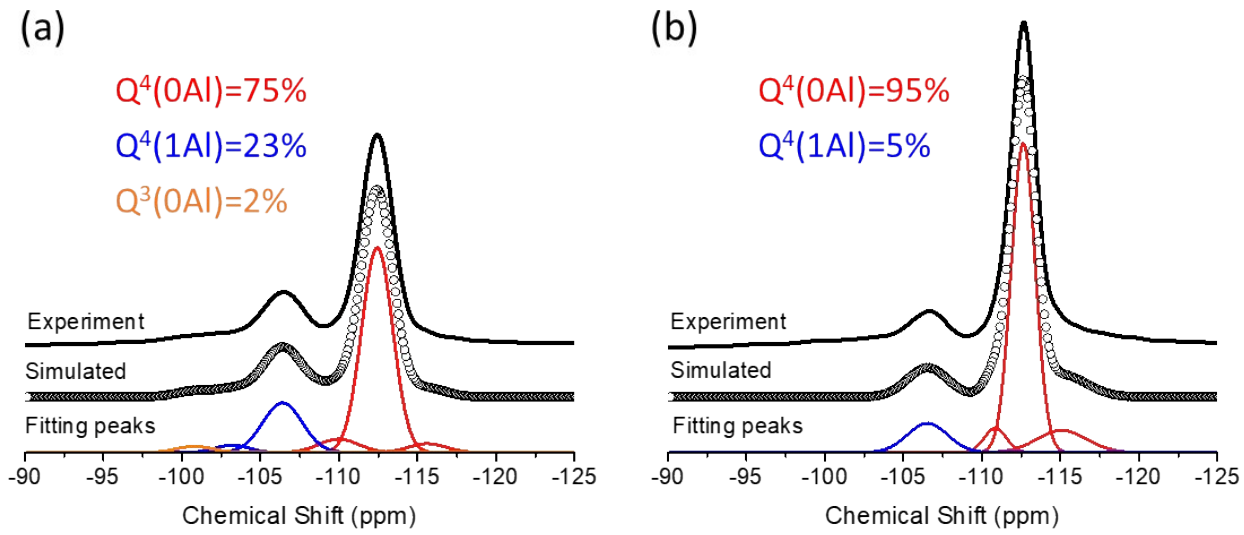

Fig. S11. Deconvolution of ^{29}Si MAS NMR patterns for (a) H-AEI-C-700 and (b) H-AEI-C-800 zeolites.

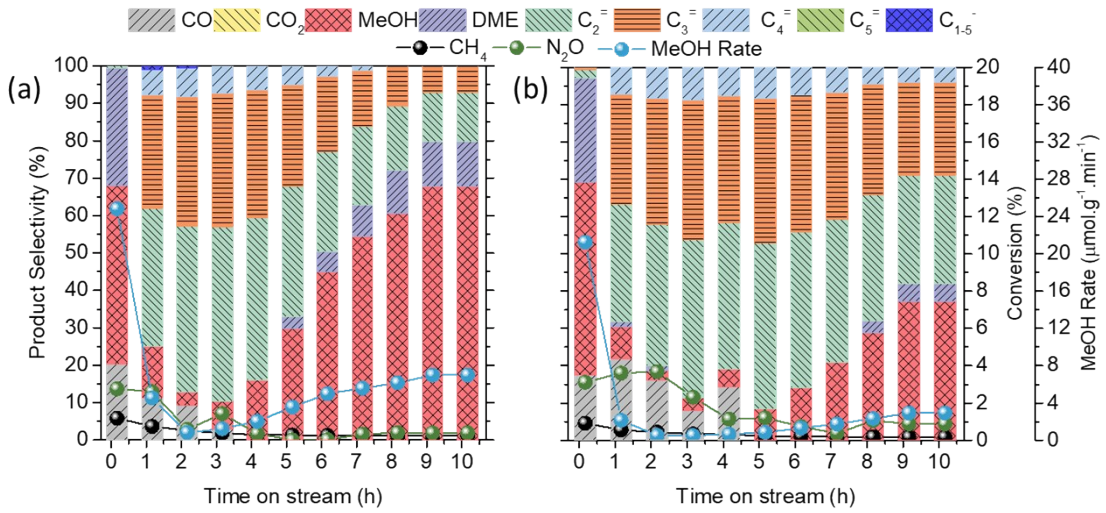

Fig. S12. Stability test of (a) 5Cu/AEI-C-700 and (b) re-prepared 5Cu/AEI-C-700 zeolite catalysts in continuous direct oxidative methane to methanol reaction at 350 °C. Reaction conditions: 100 mg catalyst, $CH_4/N_2O/H_2O/Ar$ = 10/10/2/3 ml min^{-1}, SV =15000 ml·g^{-1} h^{-1}.

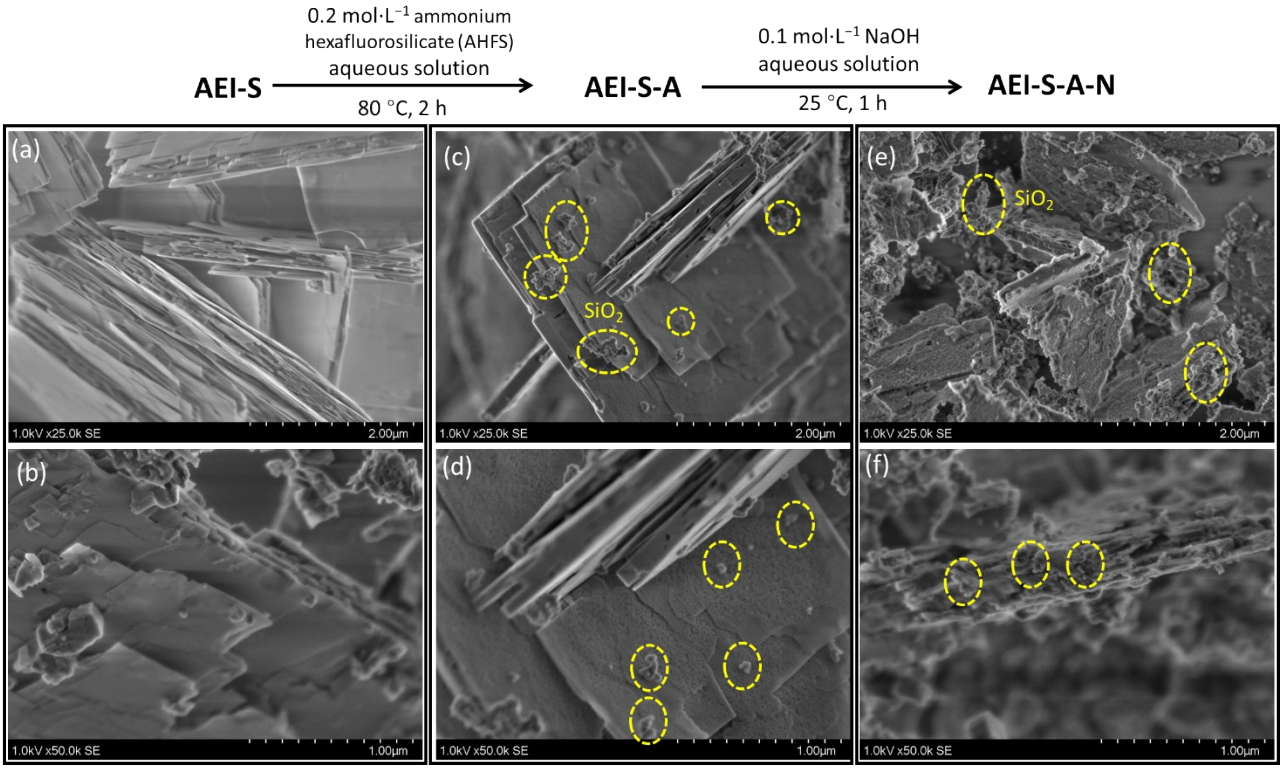

Fig. S13. SEM images of (a, b) AEI-S, (c, d) AEI-S-A, (e, f) AEI-S-A-N zeolites.

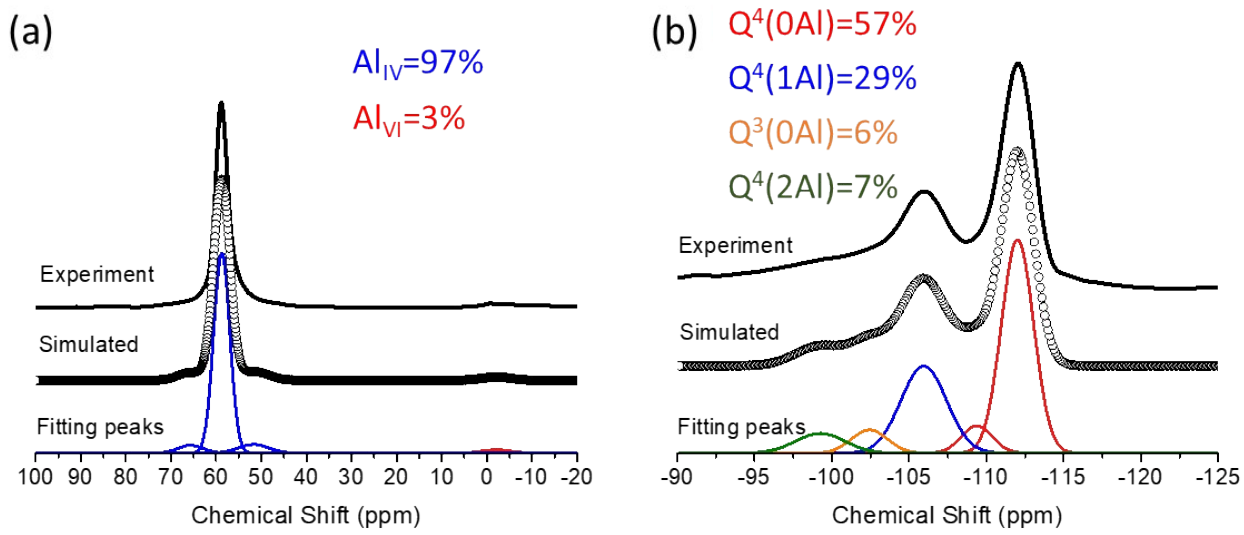

Fig. S14. Deconvolution of (a) ^{27}Al MAS NMR and (b) ^{29}Si MAS NMR pattern for H-AEI-S-A-N zeolite.

Table S1. Reaction performance of Cu/AEI zeolite catalysts in MTM at 350 °C (refer Fig. 5).

Sample	Time on stream	Conversion		Product selectivity										Formation rate
		CH_4	N_2O	CO	CO_2	MeOH	DME	$C_2^=$	$C_3^=$	$C_4^=$	C_{2-4}^-	C_5+	Aromatics	MeOH
	h	%		%										μmol·g^{-1}·min^{-1}
1Cu/AEI-C	0.2	0.9	1.2	15.7	0.0	55.7	28.1	0.6	0.0	0.0	0.0	0.0	0.0	23.5
	1.2	0.7	1.0	11.1	0.0	12.1	0.0	37.6	31.2	6.4	0.0	3.0	0.0	3.6
	2.2	0.5	1.1	6.0	0.0	1.9	0.0	47.0	35.4	7.5	0.0	3.9	0.0	0.5
	3.2	0.5	1.7	0.0	0.0	2.3	0.0	51.0	36.6	8.1	0.0	3.8	0.0	0.5
	4.2	0.4	1.1	0.0	0.0	2.2	0.0	53.3	36.1	7.5	0.0	2.5	0.0	0.4
	5.2	0.4	1.1	0.0	0.0	2.2	0.0	53.3	36.1	7.5	0.0	2.5	0.0	0.4
5Cu/AEI-C	0.2	0.7	2.6	30.8	0.0	42.9	26.3	0.0	0.0	0.0	0.0	0.0	0.0	13.0
	1.2	1.1	3.8	25.2	0.0	46.5	27.7	0.5	0.0	0.0	0.0	0.0	0.0	21.8
	2.2	1.2	2.6	29.1	0.0	45.9	24.5	0.5	0.0	0.0	0.0	0.0	0.0	24.6
	3.2	1.3	3.5	31.3	0.0	45.5	22.7	0.5	0.0	0.0	0.0	0.0	0.0	26.4
	4.2	1.2	3.5	22.2	0.0	49.1	28.1	0.6	0.0	0.0	0.0	0.0	0.0	25.2
	5.2	1.2	4.3	20.8	0.0	53.2	25.6	0.5	0.0	0.0	0.0	0.0	0.0	29.6
50Cu/AEI-C	0.2	0.8	1.8	46.6	19.1	24.3	10.0	0.0	0.0	0.0	0.0	0.0	0.0	9.2
	1.2	1.0	2.7	38.0	15.6	33.6	12.4	0.4	0.0	0.0	0.0	0.0	0.0	15.7
	2.2	1.5	3.6	43.3	21.8	24.7	9.9	0.3	0.0	0.0	0.0	0.0	0.0	17.0
	3.2	1.0	2.7	38.0	15.6	33.6	12.4	0.4	0.0	0.0	0.0	0.0	0.0	15.7
	4.2	1.5	3.6	43.3	21.8	24.7	9.9	0.3	0.0	0.0	0.0	0.0	0.0	17.0
	5.2	1.5	3.6	43.3	21.8	24.7	9.9	0.3	0.0	0.0	0.0	0.0	0.0	17.0
1Cu/AEI-S	0.2	0.8	9.3	6.7	0.0	69.0	23.8	0.4	0.0	0.0	0.0	0.0	0.0	24.5
	1.2	0.8	0.4	4.8	0.0	57.6	33.2	3.4	0.0	0.0	0.0	0.9	0.0	21.9
	2.2	0.6	0.5	9.5	0.0	7.9	0.0	37.1	35.2	7.9	1.2	2.8	0.0	2.2
	3.2	0.4	0.4	0.0	0.0	5.0	0.0	45.8	40.5	8.7	0.0	2.2	0.0	0.9
	4.2	0.4	0.4	0.0	0.0	5.0	0.0	45.8	40.5	8.7	0.0	2.2	0.0	0.9
	5.2	0.3	1.0	0.0	0.0	6.1	0.0	45.9	39.8	8.2	0.0	2.0	0.0	0.9
5Cu/AEI-S	0.2	1.0	1.9	52.4	0.0	30.7	16.3	0.6	0.0	0.0	0.0	0.0	0.0	13.3

	1.2	1.4	3.9	31.0	0.0	47.3	21.0	0.7	0.0	0.0	0.0	0.0	0.0	28.8
	2.2	1.4	3.6	25.2	0.0	49.1	24.9	0.8	0.0	0.0	0.0	0.0	0.0	29.6
	3.2	1.6	5.0	33.2	0.0	43.8	22.1	0.9	0.0	0.0	0.0	0.0	0.0	31.8
	4.2	1.6	5.0	31.0	0.0	45.4	22.8	0.9	0.0	0.0	0.0	0.0	0.0	32.5
	5.2	1.6	5.0	31.0	0.0	45.4	22.8	0.9	0.0	0.0	0.0	0.0	0.0	32.5
50Cu/AEI-S	0.2	1.0	2.8	46.0	7.1	32.9	13.7	0.3	0.0	0.0	0.0	0.0	0.0	14.9
	1.2	1.9	4.3	27.3	23.5	36.9	11.9	0.3	0.0	0.0	0.0	0.0	0.0	31.2
	2.2	1.8	3.4	26.8	23.7	34.7	14.4	0.4	0.0	0.0	0.0	0.0	0.0	27.9
	3.2	1.8	3.4	27.1	22.4	36.8	13.5	0.2	0.0	0.0	0.0	0.0	0.0	30.3
	4.2	1.8	3.4	29.0	23.4	33.4	13.9	0.2	0.0	0.0	0.0	0.0	0.0	27.2
	5.2	1.8	3.4	28.7	23.1	34.6	13.6	0.0	0.0	0.0	0.0	0.0	0.0	27.7